Polarity mechanisms such as contact inhibition of locomotion regulate persistent rotational motion of mammalian cells on micropatterns

Brian A. Camley[a,b], Yunsong Zhang[c,d], Yanxiang Zhao[b,e,f], Bo Li[b,e], Eshel Ben-Jacob[d,g], Herbert Levine[d,h,1], and Wouter-Jan Rappel[a,b]

Departments of [a]Physics and [e]Mathematics and [b]Center for Theoretical Biological Physics, University of California, San Diego, La Jolla, CA 92093; Departments of [c]Physics and Astronomy and [h]Bioengineering and [d]Center for Theoretical Biological Physics, Rice University, Houston, TX 77005; [f]Department of Mathematics, The George Washington University, Washington, DC 20052; and [g]School of Physics and Astronomy, Tel Aviv University, Tel Aviv 6997801, Israel

Pairs of endothelial cells on adhesive micropatterns rotate persistently, but pairs of fibroblasts do not; coherent rotation is present in normal mammary acini and kidney cells but absent in cancerous cells. Why? To answer this question, we develop a computational model of pairs of mammalian cells on adhesive micropatterns using a phase field method and study the conditions under which persistent rotational motion (PRM) emerges. Our model couples the shape of the cell, the cell's internal chemical polarity, and interactions between cells such as volume exclusion and adhesion. We show that PRM can emerge from this minimal model and that the cell–cell interface may be influenced by the nucleus. We study the effect of various cell polarity mechanisms on rotational motion, including contact inhibition of locomotion, neighbor alignment, and velocity alignment, where cells align their polarity to their velocity. These polarity mechanisms strongly regulate PRM: Small differences in polarity mechanisms can create significant differences in collective rotation. We argue that the existence or absence of rotation under confinement may lead to insight into the cell's methods for coordinating collective cell motility.

Collective cell migration is a crucial aspect of wound healing, growth and development of organs and tissues, and cancer invasion (1–3). Cells may move in cohesive groups ranging from small clusters of invading cancerous cells to ducts and branches during morphogenesis to monolayers of epithelial or endothelial cells. Two hallmarks of collective migration are strong cell–cell adhesion and multicellular polarity—an organization of the cellular orientation beyond the single-cell level (1). Cell–cell interactions can lead to collective behavior not evident in any single cell, including chemotaxis in clusters of cells that singly do not chemotax (4). Collective behavior may arise from cell–cell interactions altering the polarity of individual cells (5, 6). Many theories have been proposed for how this multicellular order appears, either in specific biological contexts (7–11) or in simpler, more generic models (12–16). Some authors argue that these dynamics are relatively universal and can be understood with minimal knowledge of the signaling pathways involved (2, 17).

Collective rotation is commonly observed in collectively migrating cells, especially in confinement. Persistent rotations have been observed in the slime mold *Dictyostelium discoideum* (18), canine kidney epithelial cells on adhesive micropatterns (19), and small numbers of endothelial cells on micropatterns (20, 21). Transient swirling patterns are also seen in epithelial monolayers (22). Recent work has also observed that the growth of spherical acini of human mammary epithelial cells in 3D matrix involves a coherent rotation persisting from a single cell to several cells; this rotation is not present in randomly motile cancerous cells (23). Similarly, cancerous cells on adhesive micropatterns do not develop coherent rotation (19). In a recent review of collective migration, Rørth (24) argues that "rotating movement seems to be a feature of normal epithelial cells when cultured under spatially confined conditions"; however, the origin of collective rotation and its controlling factors remain unclear.

In this paper, we study a simple example of coordinated motion: the persistent rotational motion (PRM) of small numbers of mammalian cells crawling on micropatterned substrates. Huang et al. (20) and Huang and coworkers (21) observed that pairs of endothelial cells on islands of fibronectin robustly developed PRM in a "yin–yang" shape. By contrast, fibroblasts did not rotate, developing a straight, static interface between the two cells. We develop a computational model of multiple crawling mammalian cells that couples the cells' mechanical deformations to their biochemical polarity (asymmetry in a chemical species) and includes both mechanical and chemical cell–cell interactions. We use this model as a framework to understand which mechanical and chemical factors regulate robust PRM of cells on micropatterns. This simple system can lead to new insights into cell–cell interactions and multicell polarity and potentially exclude or refine certain mechanisms previously proposed as the cause of collective migration. We also suggest that the yin–yang cell–cell interface shape may reflect the influence of the nucleus, which is often not modeled.

Model

We model physically interacting crawling cells with a chemical species ρ and a fluctuating inhibitor of ρ, I. ρ orients the cell front; I controls cell persistence. We also model four "polarity mechanisms" that reorient cell polarity (e.g., by generating I at cell–cell contact). We extend the phase field description of a crawling eukaryotic cell as studied in Shao et al. (25) to study multiple cells interacting by volume exclusion and cell–cell

Significance

During the growth of an embryo or the spreading of a tumor, cells may travel collectively. We study a computational model of a simple example of collective migration: two cells confined to a square adhesive pattern. In this confinement, some cell types rotate, whereas others do not. We model these crawling cells, the forces between them, and several possible ways that the cells could choose what direction they will crawl—their "polarity mechanism." We show that the cell polarity mechanism can control whether the pairs of cells rotate or remain fixed. This suggests that we can learn about how large groups of cells choose their direction by studying the rotation of pairs.

adhesion. The phase field method has a long history of being used to study interfacial motion problems, including cell dynamics (26–31). Our model couples biochemical polarity, modeled by reaction–diffusion equations within the cell, and mechanical forces exerted by cells, including adhesive and repulsive forces between the two cells. For simplicity, we assume the interface motion is solely driven by local forces (25), neglecting fluid flow (32, 33). We treat cells as 2D, characterized by an interface with constant line tension γ and bending modulus κ. This interface is tracked by a "phase field" $\phi(\mathbf{r})$ that smoothly varies from zero outside of the cell to unity inside it over a length scale ε. We also model the nucleus of the cell with an additional phase field $\nu(\mathbf{r})$, treating it as an object with a fixed area as well as line tension γ_{nuc} and bending modulus κ_{nuc}. The nucleus moves freely subject to the constraint that it repels and is repelled by the cell membrane; this moves it to the back of the cell, consistent with ref. 20.

We describe two chemical components within the cell. First, the chemical polarity of the cell is determined by the concentration of a Rho GTPase $\rho(\mathbf{r})$ that indicates the cell front (e.g., Rac or cdc42, an "actin promoter"). The Rho GTPase dynamics are given by a modification of the generic wave-pinning scheme of Mori et al. (34); this mechanism leads to a polarized cell with high $\rho(\mathbf{r})$ defining the front and low $\rho(\mathbf{r})$ characterizing the back of the cell. Second, we control the cell's persistence of motion as well as potential cell–cell polarity coupling by introducing a fluctuating inhibitory field $I(\mathbf{r})$ that deactivates ρ. Increasing the fluctuations of I decreases the persistence of the cell's motion (*SI Appendix*, Fig. S2).

Each cell and nucleus has a phase field $\phi^{(i)}(\mathbf{r})$, $\nu^{(i)}(\mathbf{r})$. From force balance, these obey (25) (see *SI Appendix*):

$$\partial_t \phi^{(i)}(\mathbf{r},t) = \frac{1}{\tau}\left[\alpha\chi(\mathbf{r})\rho^{(i)} - \beta\right]\left|\nabla\phi^{(i)}\right| - \frac{1}{\tau\epsilon}\frac{\delta H}{\delta\phi^{(i)}} \qquad [1]$$

$$\partial_t \nu^{(i)}(\mathbf{r},t) = -\frac{M}{\tau_{nuc}}\left(A_\nu^{(i)} - A_{nuc}\right)\left|\nabla\nu^{(i)}\right| - \frac{1}{\tau_{nuc}\epsilon}\frac{\delta H}{\delta\nu^{(i)}}. \qquad [2]$$

The first term on the right of Eq. 1 is the active motion of the membrane driven by actomyosin forces: The cell membrane is pushed radially outward at the cell front, where $\alpha\chi\rho > \beta$, but contracts at the back, where $\alpha\chi\rho < \beta$. α sets the protrusion strength, β sets the contraction strength, and τ is a friction coefficient. We hypothesize, following the logic of ref. 33, that protrusion does not occur when the cell cannot adhere to the micropattern, and therefore define $\chi(\mathbf{r})$ to be unity on the micropattern and zero off it. The second term of Eq. 1 shows that the phase field will, in the absence of actomyosin driving forces, minimize a Hamiltonian H. This energy, which will be discussed below, includes contributions from the deformation of the membrane, membrane–nucleus exclusion, and cell–cell interactions. We are modeling cells that may spread, and thus do not fix their area (see, e.g., ref. 35).

The dynamics of the cell nucleus in Eq. 2 similarly minimizes H but has no active driving force. Instead, we model the nucleus as effectively incompressible and implement a penalty term that contracts (expands) the nucleus isotropically when its area $A_\nu = \int d^2r\,\nu(\mathbf{r})$ is larger (smaller) than the prescribed area A_{nuc}. M is the strength of this penalty term and τ_{nuc} the friction coefficient for nuclear motion.

The Hamiltonian is given by

$$H = \sum_{i=1}^{n_c} H_{single\ cell}\left[\phi^{(i)}, \nu^{(i)}\right] + H_{cell-cell}, \qquad [3]$$

where $H_{single\ cell}[\phi, \nu] = H_\phi[\phi] + H_\nu[\nu] + H_{nuclear\ constraint}[\phi, \nu]$ and n_c is the number of cells. The phase-field energy for ϕ is

$$H_\phi = \gamma\int d^2r\left[\frac{\epsilon}{2}|\nabla\phi|^2 + \frac{G(\phi)}{\epsilon}\right] + \frac{\kappa}{2}\int d^2r\frac{1}{\epsilon}\left[\epsilon\nabla^2\phi - \frac{G'(\phi)}{\epsilon}\right]^2,$$

where $G(\phi) = 18\phi^2(1 - \phi)^2$ is a double-well potential that is minimized by $\phi = 0$ (cell exterior) and $\phi = 1$ (cell interior). Here, γ is the interface tension and κ its bending modulus. In the sharp-interface limit $\varepsilon \to 0$, H_ϕ becomes the usual Canham–Helfrich Hamiltonian (36, 37) for a fluid membrane (see refs. 38 and 39). H_ν is given by an identical form with ϕ replaced by ν and different parameters γ_{nuc} and κ_{nuc}. We model the cell–nucleus interaction by imposing a simple energy penalty if the nucleus begins to exit the cell, $H_{nuclear\ constraint} = g_{nuc}\int d^2r[1 - \phi(\mathbf{r})]\nu(\mathbf{r})$. We model two physical cell–cell interactions, a repulsion between cell bodies and an attraction between cell interfaces, using a variant of the method of Nonomura (40). Excluded volume is modeled by penalizing cell overlap, and the adhesion interaction promotes membrane–membrane contact between cells.

$$H_{cell-cell} = \sum_{i\neq j}\int d^2r\left[\frac{g}{2}\phi^{(i)}(\mathbf{r})\phi^{(j)}(\mathbf{r}) - \frac{\sigma\epsilon^3}{4}\left|\nabla\phi^{(i)}\right|^2\left|\nabla\phi^{(j)}\right|^2\right]$$

g penalizes overlap area between the two cells. σ controls the energy of adhesion but is not precisely the energy of adhesion per length of overlap (*SI Appendix*).

We model chemical concentrations within the cell with reaction–diffusion equations. To solve these equations in the moving and deforming cell interior, we use the phase field method (25, 26, 30), which has numerically and analytically been shown to reproduce reaction–diffusion dynamics with no-flux boundary conditions (26, 30). Our equations for the Rho GTPase ρ and the fluctuating inhibitor I in each cell are

$$\partial_t\left(\phi^{(i)}\rho^{(i)}\right) = \nabla\cdot\left[\phi^{(i)}D_\rho\nabla\rho^{(i)}\right] + \phi f_\rho\left(\rho^{(i)}, \rho_{cyt}^{(i)}, I^{(i)}\right), \qquad [4]$$

$$\partial_t\left(\phi^{(i)}I^{(i)}\right) = \nabla\cdot\left[\phi^{(i)}D_I\nabla I^{(i)}\right] + \phi f_I\left(I^{(i)}, \{\phi\}, \{\rho\}\right), \qquad [5]$$

where $D_{\rho,I}$ are diffusion coefficients and $f_{\rho,I}$ are reaction terms. f_ρ describes an exchange between active, membrane-bound Rho GTPase, $\rho(\mathbf{r})$ and a uniform cytosolic pool ρ_{cyt}; $\rho(\mathbf{r})$ actively recruits cytosolic Rho GTPase, and positive (negative) I increases (decreases) the transition rate of $\rho \to \rho_{cyt}$. This model, a variant of the generic scheme proposed by Mori et al. (34), can create a steady-state distribution of ρ such that one side of the cell (the front) has high ρ and the other side has low ρ. f_I includes a spatially
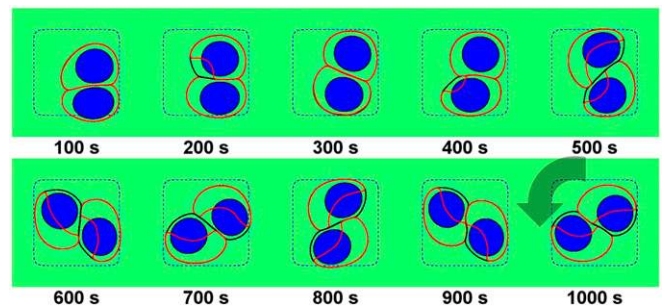
Fig. 1. Persistent rotational motion can be recreated in our minimal model. Parameters are listed in *SI Appendix*; $L_{micro} = 30$ μm. In this figure, and throughout the paper, the cell membrane is indicated by a black line, the Rho GTPase ρ by a red contour showing the points where $\rho = \max(\rho\phi)/2$, the cell nucleus by a blue shape, and the micropattern by a blue dashed line (*SI Appendix*, Fig. S1 provides a legend). See also Movie S1.

and temporally uncorrelated noise as well as a decay of I over time. We will also use the term f_I to model couplings between cell–cell contact and polarity. For instance, we will model "contact inhibition of locomotion" in which cell–cell contact locally generates I. The full reaction terms are shown in *SI Appendix*.

Results

Pairs of Confined Cells Can Develop Persistent Rotation but Also May Stall. In our simulations of pairs of cells on a square micropattern we can observe PRM in a minimal model without explicit cell–cell alignment interactions (Fig. 1). To observe rotation, we have chosen the parameters of the model such that the cells are highly persistent and are strongly adherent. We also set parameters such that cell spread area is smaller than the micropattern, so free- and confined-cell morphologies are similar. Parameters are listed in *SI Appendix*, Table S1.

In Fig. 1, we show a simulation where our cells develop PRM, but other results occur, even with identical parameters. In Fig. 2, we show representative snapshots of simulations with different initial conditions. We find rotational motion in only 5/30 cases (see *SI Appendix* for distribution of initial conditions). Non-rotating cell pairs have two common morphologies: cells stuck in either opposing corners of the micropattern or a single corner; we also see transient cases with one or more cell unpolarized and one case of rotation stopping (Movie S1). PRM is completely inhibited on smaller micropatterns ($L_{micro} = 25$ μm); in this case, the cell spread area is constricted, preventing polarization (33, 34, 42).

Rotational Motion Is Strongly Regulated by Cell Polarity Mechanisms. In our studies of PRM above, we assumed that the presence of the other cells does not directly influence the underlying chemical polarity of any cell, except via mechanical interactions. This minimal model creates a persistent cohort rotation (although not robustly). However, the existence of direct interactions between the polarity of neighboring cells has been well established, including contact inhibition of locomotion in neural crest cells and fibroblasts (3–5, 43, 44) and polarity induced by stress on cadherin adhesions of mesendoderm cells (6). We argue that effects of this type must be included in realistic models of PRM. Many polarity-regulating mechanisms have also been shown to create collective cell migration in simulations. These include extensions of flocking models of birds in which cell polarity (and hence velocity) become aligned with cell neighbor velocities (11, 14, 18, 45), models where polarity becomes aligned with the cell's velocity or displacement (13, 15, 17, 46–48), and more directly experimentally inspired mechanisms including contact inhibition of locomotion (10, 12). We are interested in studying the role of these polarity-control mechanisms in establishing persistent rotation and cohort migration in these small systems, which may provide a useful testing ground for effects beyond the more universal features of alignment in larger systems.

We implement within our cell model four generic types of polarity-alignment mechanisms (Fig. 3): (*i*) neighbor alignment

(NA), in which cells align their polarity to the average velocity of the cells in the neighborhood (e.g. 14, 18, 45); (*ii*) velocity alignment (VA), in which cells align their polarity to their own velocity (13, 15, 47, 48); (*iii*) contact inhibition of locomotion (CIL), in which cell polarity is inhibited by contact with other cells (10, 12); and (*iv*) cell front–front inhibition (FF), a generalization of CIL in which only contact with the cell front is inhibitory. FF is supported by experiments of Desai et al. (49) that show head–head collisions lead to repolarization at a greater rate than head–tail collisions. There is also some historical precedent; in early papers on CIL, Abercrombie and Dunn (44) argued for a distinction between head–head and head–tail collisions; see also ref. 43 for a discussion of this point. For details of the implementation of these polarity types, see *SI Appendix*.

In Fig. 3 we present simulations of pairs of cells with these four different polarity mechanisms. We discover that of these four generic models VA robustly promotes the presence of PRM, CIL completely eliminates rotation, and NA promotes the linear motion of cells in an aligned flock but inhibits PRM. FF promotes PRM, but only if the cells are sufficiently confined ($L_{micro} = 25$ μm); in micropatterns with $L_{micro} = 30$ μm, the FF mechanism leads to static cells. These general trends persist even if our parameters are varied, unless cell motility is inhibited by the parameter changes (*SI Appendix*, Tables S2–S5 and Fig. S7); complete loss of cell–cell adhesion also disrupts PRM in FF (*SI Appendix*, Fig. S7C).

CIL generates the inhibitor $I(\mathbf{r})$ at cell–cell contact. In Fig. 3, we see that the $I(\mathbf{r})$ at the cell interface ensures that the cells polarize directly away from one another, preventing any rotation. As the cells remain in contact, $I(\mathbf{r})$ is still generated at the interface, ensuring that the cells maintain their polarity pointing away from the contact.

FF cells initially resemble CIL cells, but when the front of one cell touches the back of another the chiral symmetry of the pair is broken, leading to rotation. However, in the $L_{micro} = 30$ μm micropattern, FF cells cannot effectively make and maintain this symmetry-breaking contact, and the FF mechanism actually suppresses PRM (*SI Appendix*, Fig. S3).

NA cells are successful at creating a sort of collective motion—they do remain aligned with each other. However, the strong alignment between cells prevents the development of PRM. Instead, pairs of NA cells travel as a "flock," moving from one side of the pattern to the other, then reversing. This is relatively unsurprising, because the NA mechanism is commonly used to describe flocking of birds (14). Similar mechanisms can, however, create collective rotation in a larger collection of cells, where local alignment is compatible with rotation (18).

When the VA mechanism is imposed, cells impact the boundary and then reorient, because their velocity is no longer outwardly directed; this reorientation ensures that cells do not become trapped at the boundary, as occurs in the default mechanism. PRM occurs in VA cells in both 25-μm and 30-μm micropatterns. However, "flocking" motions are also seen (transiently in 25-μm patterns and occasionally in 30-μm patterns; Movies S6 and S10); flocking can be suppressed by increasing the noise strength ζ (Movie S11).

Rotational Motion Is Disrupted in Cells with Lower Persistence. We have shown that the presence and robustness of PRM can be controlled by polarity-alignment mechanisms. However, persistent rotational motion also requires that the cell's linear motion be sufficiently persistent; as the model of Huang et al. (20) makes clear, cells that undergo effectively pure random-walk motility are not likely to develop rotation. In our model, the persistence time (as measured from the cell's velocity–velocity correlation function) is controlled by the amplitude of the fluctuating source term in the $I(\mathbf{r})$ equation. We show in *SI Appendix*, Fig. S4 and Movie S12 that decreasing cell persistence also disrupts persistent motion in our model, as expected.
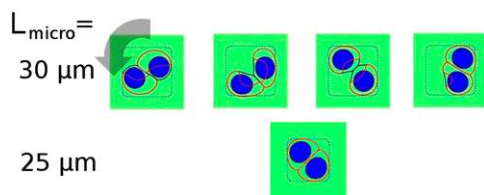
Fig. 2. PRM with the minimal model is not robust, and does not exist on small micropatterns. We show typical states of our simulation of two confined cells at 1,000 s. (*Upper*) Micropattern size $L_{micro} = 30$ μm. (*Lower*) Micropattern size $L_{micro} = 25$ μm. See also Movies S1 and S2.
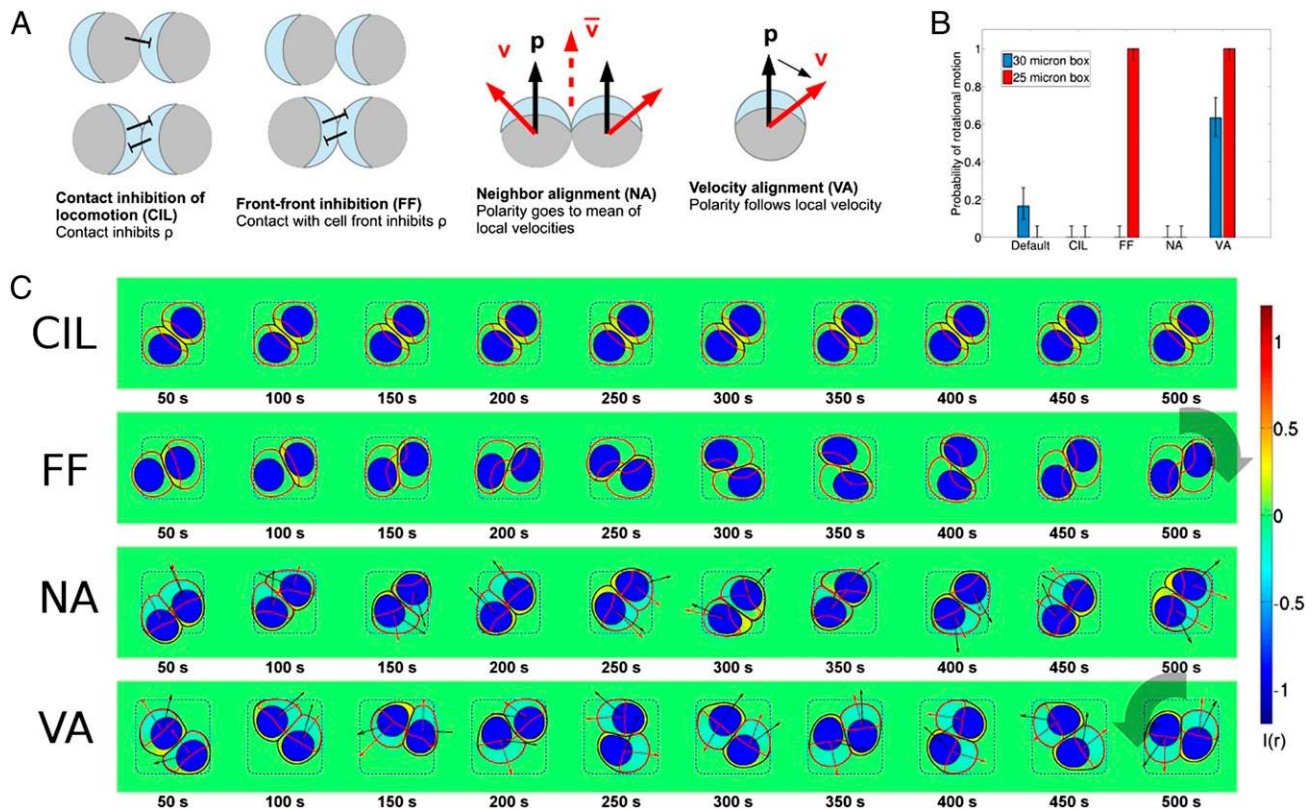
Fig. 3. Polarity mechanisms can control persistent rotational motion. (*A*) We implement four distinct mechanisms for cell polarity. In CIL cell contact locally generates $I(\mathbf{r})$, inhibiting ρ. In FF, $I(\mathbf{r})$ is generated when a cell contacts another cell's front. Here, ρ is indicated by light blue at the front of the cell. In the NA and VA mechanisms, we introduce an auxiliary polarity vector $\hat{\mathbf{p}}$ with its own equation of motion. NA orients $\hat{\mathbf{p}}$ to the local average of velocities in its neighborhood $\bar{\mathbf{v}}$ with a timescale T_{orient}; this resembles flocking-inspired models. VA orients $\hat{\mathbf{p}}$ along the cell's velocity with a timescale T_{orient}. In both of these models the cell's chemical polarity is then biased to orient the front of the cell (high ρ) with the polarity $\hat{\mathbf{p}}$. There is also a noise term; $\hat{\mathbf{p}}$ fluctuates around its target direction. Details of the implementation of these models are described in *SI Appendix*. (*B*) PRM probability is controlled by polarity mechanisms; error bars are 68% confidence intervals by the method of ref. 50. "Default" indicates the minimal model with no polarity mechanism. (*C*) Representative time traces are shown for different polarity mechanisms. Micropattern size $L_{micro} = 25$ μm. As above, cell boundary is shown as a black line, $\rho(\mathbf{r})$ by its contour (in red), the nucleus by a blue shape, and $I(\mathbf{r})$ by the color map. In VA and NA mechanisms cell velocity is shown as a red arrow, and the polarity vector $\hat{\mathbf{p}}$ as a black arrow. See also Movies S3–S11 and *SI Appendix*, Fig. S3.

Extensions to Different Geometries and Numbers of Cells. It is straightforward to extend our method to different geometries, simply by changing the function $\chi(\mathbf{r})$ that describes the adhesive micropattern. It is in principle also simple to increase the number of cells, although the computational expense increases significantly, and smaller time steps may be required to deal with the added extent of cell–cell adhesion. New, more complex dynamics may also appear when the number of cells increases, including changes in cell contact topology (e.g., as studied in ref. 51). We show snapshots of two cells and three cells persistently rotating within circular micropatterns as well as three cells rotating within a square micropattern in *SI Appendix*, Fig. S5.

Discussion
In our simulation, the shape of the interface between two rotating cells can be strongly influenced by the presence of a nucleus, including changing its chirality (*SI Appendix*, Fig. S6). Huang et al. (20) and Huang and coworkers (21) observed experimentally that, in a pair of rotating cells, the chirality of the cell interface correlates with the direction of the cell motion (fig. 3*A* in ref. 20). However, the direction of this motion is somewhat counterintuitive (52). If one cell's lamellipodium is pushing on the rear of another cell, it would be natural to assume that the rear of the cell curves inward, but this does not occur. Leong (52) presented a dissipative particle dynamics model of two cells displaying PRM with an interface shape consistent with

experiment. However, this model treats cells as permanently attached to one another and cannot explain how two-cell dynamics arises from single-cell properties. In particular, it is not clear how single-cell persistence appears in Leong's model, or whether an individual cell would develop a polarity. In addition, the model of Leong does not have a nucleus, which may by itself alter the interface curvature. Because interface shape depends on the presence of a nucleus, interface shape may be sensitive to active positioning of the nucleus (53) or rheological details of the cell (54) we have not modeled. Even within our simple model many different parameters, including the micropattern size and the polarity mechanism, may affect the interface shape, and the precise interface shape in PRM is not a robust prediction of our model (*SI Appendix*, Fig. S6), although we expect the influence of the nucleus to remain important. The nuclear effect could be tested by studying PRM of cell types with smaller nuclei or nuclei-free cell fragments (55). PRM in keratocytes and keratocyte fragments may be particularly interesting because our results suggest that even with highly persistent crawling objects, such as keratocytes and fragments, persistent motion may not be robust in the absence of a coordinating mechanism. In addition to the absence of a nucleus, cell–cell adhesion and polarity mechanisms may differ between fragments and keratocytes. If so, keratocytes and keratocyte fragments may differ in both their interface shape and in the robustness of PRM.

PHYSICS

CELL BIOLOGY

Our simulations provide insight into the crucial features regulating the existence and robustness of PRM in cell pairs, which we view as the simplest possible collective motion. Our simulations show that seemingly subtle differences between polarity mechanisms can have significant effects on PRM, and that these differences are robust to changes in many model parameters. The mechanisms of CIL and FF are very similar and may be difficult to distinguish from unconstrained collision data (5). In adhesive stripe assays, collision statistics are simpler to obtain (43, 49); Desai et al. (49) note that head–tail collisions are less likely to lead to repolarization of both cells, consistent with FF rather than our CIL mechanism. However, other mechanisms, such as VA, could also lead to both PRM and asymmetry between head–head and head–tail collisions. These mechanisms may be able to be distinguished using the results of Scarpa et al. (43) and Desai et al. (49). Chiral bias from micropattern shape (56) or intrinsic cell chirality (57) may also be incorporated into our model.

Polarity mechanisms have a strong interplay with confinement. For cells on a 30-μm square, the FF mechanism inhibits PRM, whereas for cells on a 25-μm square FF creates PRM robustly. By contrast, without an explicit polarity mechanism, our model cells cannot polarize on a 25-μm square, and PRM is inhibited. The dependence of cell's ability to polarize on cell size is a feature of the minimal polarity model of Mori et al. (34), and if this model is changed, we would expect details of the polarity–confinement interaction to change. A variety of more complicated and biologically specific polarity models for crawling cells have also been developed (58–62). Many of these models could be implemented within our framework, and we would expect them to alter the development of PRM to some extent; within recent simulations, the details of the chemical feedbacks alter the ability of the cell to coherently choose a direction when encountering a barrier (62).

The presence or absence of PRM can indicate cell type [endothelial or fibroblast (20), although rotation is seen in larger collections of fibroblasts (57)] or mutation [normal or cancerous (19, 23)]. Huang et al. (20) claim these motions are characteristic of the persistence of the cell motion, and our simulations agree that decreasing cell persistence inhibits PRM. However, we emphasize the role that polarity mechanisms play in coordinating PRM; FF or VA can change our model from displaying 0% PRM to 100% PRM. This suggests that cell polarity mechanism, rather than cell persistence, may distinguish cell types that display PRM and those that do not. Some aspects of CIL are known to differ between normal and malignant cells (63, 64). It may be possible to test the relevant factors by altering cell persistence (65, 66). If the primary regulator of PRM is the cell polarity mechanism, studying PRM provides insight into collective cell migration, where much larger numbers of cells regulate their polarity to move effectively as a group. In particular, our results suggest that contact inhibition of locomotion as modeled here is not a likely cause of collective migration, but that modifications such as front–front inhibition could lead to robust collective motion.

1. Friedl P, Gilmour D (2009) Collective cell migration in morphogenesis, regeneration and cancer. *Nat Rev Mol Cell Biol* 10(7):445–457.
2. Vedula SR, Ravasio A, Lim CT, Ladoux B (2013) Collective cell migration: A mechanistic perspective. *Physiology (Bethesda)* 28(6):370–379.
3. Theveneau E, Mayor R (2013) Collective cell migration of epithelial and mesenchymal cells. *Cell Mol Life Sci* 70:3481–3492.
4. Theveneau E, et al. (2010) Collective chemotaxis requires contact-dependent cell polarity. *Dev Cell* 19(1):39–53.
5. Carmona-Fontaine C, et al. (2008) Contact inhibition of locomotion in vivo controls neural crest directional migration. *Nature* 456(7224):957–961.
6. Weber GF, Bjerke MA, DeSimone DW (2012) A mechanoresponsive cadherin-keratin complex directs polarized protrusive behavior and collective cell migration. *Dev Cell* 22(1):104–115.
7. Burak Y, Shraiman BI (2009) Order and stochastic dynamics in Drosophila planar cell polarity. *PLOS Comput Biol* 5(12):e1000628.
8. Salbreux G, Barthel LK, Raymond PA, Lubensky DK (2012) Coupling mechanical deformations and planar cell polarity to create regular patterns in the zebrafish retina. *PLOS Comput Biol* 8(8):e1002618.
9. Amonlirdviman K, et al. (2005) Mathematical modeling of planar cell polarity to understand domineering nonautonomy. *Science* 307(5708):423–426.
10. Vedel S, Tay S, Johnston DM, Bruus H, Quake SR (2013) Migration of cells in a social context. *Proc Natl Acad Sci USA* 110(1):129–134.
11. Sepúlveda N, et al. (2013) Collective cell motion in an epithelial sheet can be quantitatively described by a stochastic interacting particle model. *PLOS Comput Biol* 9(3):e1002944.
12. Coburn L, Cerone L, Torney C, Couzin ID, Neufeld Z (2013) Tactile interactions lead to coherent motion and enhanced chemotaxis of migrating cells. *Phys Biol* 10(4):046002.
13. Szabó B, et al. (2006) Phase transition in the collective migration of tissue cells: Experiment and model. *Phys Rev E Stat Nonlin Soft Matter Phys* 74(6 Pt 1):061908.
14. Vicsek T, Zafeiris A (2012) Collective motion. *Phys Rep* 517(3):71–140.
15. Basan M, Elgeti J, Hannezo E, Rappel W-J, Levine H (2013) Alignment of cellular motility forces with tissue flow as a mechanism for efficient wound healing. *Proc Natl Acad Sci USA* 110(7):2452–2459.
16. Gov NS (2009) Traction forces during collective cell motion. *HFSP J* 3(4):223–227.
17. Kabla AJ (2012) Collective cell migration: Leadership, invasion and segregation. *J R Soc Interface* 9(77):3268–3278.
18. Rappel W-J, Nicol A, Sarkissian A, Levine H, Loomis WF (1999) Self-organized vortex state in two-dimensional Dictyostelium dynamics. *Phys Rev Lett* 83(6):1247–1250.
19. Doxzen K, Vedula SRK, Leong MC, Hirata H, Gov N, Kabla AJ, Ladoux B, Lim CT (2013) Guidance of collective cell migration by substrate geometry. *Integr Biol* 5:1026–1035.
20. Huang S, Brangwynne CP, Parker KK, Ingber DE (2005) Symmetry-breaking in mammalian cell cohort migration during tissue pattern formation: Role of random-walk persistence. *Cell Motil Cytoskeleton* 61(4):201–213.
21. Brangwynne C, Huang S, Parker KK, Ingber DE, Ostuni E (2000) Symmetry breaking in cultured mammalian cells. *In Vitro Cell Dev Biol Anim* 36(9):563–565.
22. Angelini TE, et al. (2011) Glass-like dynamics of collective cell migration. *Proc Natl Acad Sci USA* 108(12):4714–4719.
23. Tanner K, Mori H, Mroue R, Bruni-Cardoso A, Bissell MJ (2012) Coherent angular motion in the establishment of multicellular architecture of glandular tissues. *Proc Natl Acad Sci USA* 109(6):1973–1978.
24. Rørth P (2012) Fellow travellers: Emergent properties of collective cell migration. *EMBO Rep* 13(11):984–991.
25. Shao D, Rappel W-J, Levine H (2010) Computational model for cell morphodynamics. *Phys Rev Lett* 105(10):108104.
26. Kockelkoren J, Levine H, Rappel W-J (2003) Computational approach for modeling intra- and extracellular dynamics. *Phys Rev E Stat Nonlin Soft Matter Phys* 68(3 Pt 2):037702.
27. Boettinger WJ, Warren JA, Beckermann C, Karma A (2002) Phase-field simulation of solidification 1. *Annu Rev Mater Res* 32(1):163–194.
28. Collins JB, Levine H (1985) Diffuse interface model of diffusion-limited crystal growth. *Phys Rev B Condens Matter* 31(9):6119–6122.
29. Ziebert F, Swaminathan S, Aranson IS (2012) Model for self-polarization and motility of keratocyte fragments. *J R Soc Interface* 9(70):1084–1092.
30. Li X, Lowengrub J, Rätz A, Voigt A (2009) Solving PDEs in complex geometries: A diffuse domain approach. *Commun Math Sci* 7(1):81–107.
31. Marth W, Voigt A (2013) Signaling networks and cell motility: A computational approach using a phase field description. *J Math Biol* 69(1):91–112.
32. Shao D, Levine H, Rappel W-J (2012) Coupling actin flow, adhesion, and morphology in a computational cell motility model. *Proc Natl Acad Sci USA* 109(18):6851–6856.
33. Camley BA, Zhao Y, Li B, Levine H, Rappel WJ (2013) Periodic migration in a physical model of cells on micropatterns. *Phys Rev Lett* 111(15):158102.
34. Mori Y, Jilkine A, Edelstein-Keshet L (2008) Wave-pinning and cell polarity from a bistable reaction-diffusion system. *Biophys J* 94(9):3684–3697.
35. Albert PJ, Schwarz US (2014) Dynamics of cell shape and forces on micropatterned substrates predicted by a cellular Potts model. *Biophys J* 106(11):2340–2352.
36. Helfrich W (1973) Elastic properties of lipid bilayers: Theory and possible experiments. *Z Naturforsch C* 28(11):693–703.
37. Canham PB (1970) The minimum energy of bending as a possible explanation of the biconcave shape of the human red blood cell. *J Theor Biol* 26(1):61–81.
38. Li B, Zhao Y (2013) Variational implicit solvation with solute molecular mechanics: from diffuse-interface to sharp-interface models. *SIAM J Appl Math* 73(1):1–23.
39. Röger M, Schätzle R (2006) On a modified conjecture of De Giorgi. *Math Z* 254(4):675–714.
40. Nonomura M (2012) Study on multicellular systems using a phase field model. *PLoS ONE* 7(4):e33501.
41. Doyle AD, Wang FW, Matsumoto K, Yamada KM (2009) One-dimensional topography underlies three-dimensional fibrillar cell migration. *J Cell Biol* 184(4):481–490.
42. Mori Y, Jilkine A, Edelstein-Keshet L (2011) Asymptotic and bifurcation analysis of wave-pinning in a reaction-diffusion model for cell polarization. *SIAM J Appl Math* 71(4):1401–1427.

43. Scarpa E, et al. (2013) A novel method to study contact inhibition of locomotion using micropatterned substrates. *Biol Open* 2(9):901–906.
44. Abercrombie M, Dunn GA (1975) Adhesions of fibroblasts to substratum during contact inhibition observed by interference reflection microscopy. *Exp Cell Res* 92(1):57–62.
45. Vicsek T, Czirók A, Ben-Jacob E, Cohen I, Shochet O (1995) Novel type of phase transition in a system of self-driven particles. *Phys Rev Lett* 75(6):1226–1229.
46. Szabó A, et al. (2010) Collective cell motion in endothelial monolayers. *Phys Biol* 7(4):046007.
47. Henkes S, Fily Y, Marchetti MC (2011) Active jamming: Self-propelled soft particles at high density. *Phys Rev E Stat Nonlin Soft Matter Phys* 84(4 Pt 1):040301.
48. Camley BA, Rappel WJ (2014) Velocity alignment leads to high persistence in confined cells. *Phys Rev E Stat Nonlin Soft Matter Phys* 89(6-1):062705.
49. Desai RA, Gopal SB, Chen S, Chen CS (2013) Contact inhibition of locomotion probabilities drive solitary versus collective cell migration. *J R Soc Interface* 10(88):20130717.
50. Clopper CJ, Pearson ES (1934) The use of confidence or fiducial limits illustrated in the case of the binomial. *Biometrika* 26(4):404–413.
51. Bi D, Lopez JH, Schwarz JM, Manning ML (2014) Energy barriers and cell migration in densely packed tissues. *Soft Matter* 10(12):1885–1890.
52. Leong FY (2013) Physical explanation of coupled cell-cell rotational behavior and interfacial morphology: A particle dynamics model. *Biophys J* 105(10):2301–2311.
53. Gundersen GG, Worman HJ (2013) Nuclear positioning. *Cell* 152(6):1376–1389.
54. Wirtz D (2009) Particle-tracking microrheology of living cells: Principles and applications. *Annu Rev Biophys* 38:301–326.
55. Verkhovsky AB, Svitkina TM, Borisy GG (1999) Self-polarization and directional motility of cytoplasm. *Curr Biol* 9(1):11–20.
56. Kushiro K, Chang S, Asthagiri AR (2010) Reprogramming directional cell motility by tuning micropattern features and cellular signals. *Adv Mater* 22(40):4516–4519.
57. Wan LQ, et al. (2011) Micropatterned mammalian cells exhibit phenotype-specific left-right asymmetry. *Proc Natl Acad Sci USA* 108(30):12295–12300.
58. Lin B, et al. (2012) Synthetic spatially graded Rac activation drives cell polarization and movement. *Proc Natl Acad Sci USA* 109(52):E3668–E3677.
59. Edelstein-Keshet L, Holmes WR, Zajac M, Dutot M (2013) From simple to detailed models for cell polarization. *Phil Trans R Soc B* 368(1629):20130003.
60. Holmes WR, Carlsson AE, Edelstein-Keshet L (2012) Regimes of wave type patterning driven by refractory actin feedback: Transition from static polarization to dynamic wave behaviour. *Phys Biol* 9(4):046005.
61. Holmes WR, Lin B, Levchenko A, Edelstein-Keshet L (2012) Modelling cell polarization driven by synthetic spatially graded Rac activation. *PLOS Comput Biol* 8(6):e1002366.
62. Marée AF, Grieneisen VA, Edelstein-Keshet L (2012) How cells integrate complex stimuli: The effect of feedback from phosphoinositides and cell shape on cell polarization and motility. *PLOS Comput Biol* 8(3):e1002402.
63. Mayor R, Carmona-Fontaine C (2010) Keeping in touch with contact inhibition of locomotion. *Trends Cell Biol* 20(6):319–328.
64. Abercrombie M (1979) Contact inhibition and malignancy. *Nature* 281(5729):259–262.
65. Dang I, et al. (2013) Inhibitory signalling to the Arp2/3 complex steers cell migration. *Nature* 503(7475):281–284.
66. Kim D-H, Cho S, Wirtz D (2014) Tight coupling between nucleus and cell migration through the perinuclear actin cap. *J Cell Sci* 127(Pt 11):2528–2541.

PHYSICS

CELL BIOLOGY